Chinese Chemical Letters 37 (2026) 111378

Contents lists available at ScienceDirect

Chinese Chemical Letters

journal homepage: www.elsevier.com/locate/cclet

Pore surface engineering of hydrazone-linked covalent organic framework with tailor-made chelating sites for uranium extraction from seawater

Junjie Yu[a,b], Yichen Huang[a,c], Pengcheng Zhang[a], Shusen Chen[d], Yan Song[d], Congzhi Wang[a], Zijie Li[a], Liyong Yuan[a], Jipan Yu[a,*], Nannan Wang[b,*], Weiqun Shi[a,e,*]

[a] Laboratory of Nuclear Energy Chemistry, Institute of High Energy Physics, Chinese Academy of Sciences, Beijing 100049, China
[b] State Key Laboratory of Featured Metal Materials and Life-Cycle Safety for Composite Structures, MOE Key Laboratory of New Processing Technology for Nonferrous Metals and Materials, and School of Resources, Environment and Materials, Guangxi University, Nanning 530004, China
[c] School of Chemistry and Chemical Engineering, University of South China, Hengyang 421001, China
[d] CNNC Key Laboratory on Uranium Extraction from Seawater, Beijing Research Institute of Chemical Engineering and Metallurgy, Beijing 101149, China
[e] Institute of Nuclear Fuel cycle and Materials, School of Mechanical Engineering, Shanghai Jiao Tong University, Shanghai 200240, China

ARTICLE INFO

Article history:
Received 17 March 2025
Revised 12 May 2025
Accepted 26 May 2025
Available online 29 May 2025

Keywords:
Covalent organic framework
Uranium extraction from seawater
Adsorption and separation
Thiol-ene click reaction
Post-modification

ABSTRACT

The extraction of uranium from seawater is essential for the sustainable development of the nuclear industry. Covalent organic frameworks (COFs) exhibit significant potential in uranium extraction from seawater due to their high stability, designability, and large specific surface area. Herein, a vinyl-decorated covalent organic framework, designated as COF-IHEP5, was synthesized through acid-catalyzed solvothermal method. COF-IHEP5-COOH was constructed by post-modification strategy through the "thiol-ene" click reaction, where COF-IHEP5-COOH contains hydrazone-carbonyl and flexible carboxylic acid chelating sites on pore wall. This modification facilitates synergistic adsorption of uranium by utilizing a "nano trap" that is embedded within the COF framework. The maximum adsorption capacity of the post-modified COF-IHEP5-COOH for UO_2^{2+} has reached 543.8 mg/g, representing a 1.5-fold increase compared to the unmodified COF-IHEP5. Additionally, COF-IHEP5-COOH demonstrates an extraction efficiency of approximately 80 % for uranium from spiked natural seawater, featuring 4.5 times higher selectivity than vanadium. The DFT calculation results show that the adsorption of uranium orginated from the synergistic coordination of the skeleton in COF-IHEP5-COOH and carboxyl group on the side arm. This research highlights the remarkable potential of pore surface engineering in customizing active adsorption sites and offers new insights for the design of functionalized uranium adsorbents with superior binding affinity and adsorption capacities.

© 2025 Published by Elsevier B.V. on behalf of Chinese Chemical Society and Institute of Materia Medica, Chinese Academy of Medical Sciences.

One of the significant challenges facing human society in the 21st century is deep decarbonization and sustainable clean energy [1]. Traditional non-renewable energy sources, such as coal and oil, are becoming increasingly scarce, and their use inevitably results in environmental pollution. To replace fossil fuels, clean energy sources, including solar, wind, hydro, geothermal, and tidal energy, have been widely developed [2,3]. However, these sources still present numerous shortcomings and limitations regarding practicality, universality, economic viability, and technical feasibility. In contrast, nuclear energy, which has several advantages such as high energy density, stable and continuous power supply, and low carbon emissions, is widely regarded as a mature and safe technology. The growth and advancement of the nuclear industry have made a significant contribution to the demand for clean energy [4].

Uranium resources are essential for the sustainable development of the nuclear industry [5]. Nevertheless, natural uranium abundance on land is limited and challenging to extract. In contrast, the total uranium reserves in seawater are estimated to be approximately 4.5 billion tons, which is roughly 1000 times greater than the known uranium ore reserves on land [6]. Uranium reserves in seawater are sufficient to support the long-term and stable operation of nuclear power. Furthermore, uranium extraction from seawater provides a substantial resource without causing environmental pollution [7]. Consequently, there is an urgent need

* Corresponding authors.
E-mail addresses: yujipan@ihep.ac.cn (J. Yu), wangnannan@gxu.edu.cn (N. Wang), shiwq@sjtu.edu.cn (W. Shi).

https://doi.org/10.1016/j.cclet.2025.111378
1001-8417/© 2025 Published by Elsevier B.V. on behalf of Chinese Chemical Society and Institute of Materia Medica, Chinese Academy of Medical Sciences.

to develop new materials and technologies for extracting uranium from seawater to meet the growing demand for uranium resources. The extraction of uranium at extremely low concentrations from the vast ocean necessitates a cost-effective and efficient method. Among established chemical separation technologies, adsorption has been recognized as an effective, versatile, and environmentally friendly extraction method [8]. The research and development of adsorbent materials have been made for the uranium extraction from seawater [9–11]. However, the complex conditions in seawater, characterized by high ionic strength, various interfering ions, extremely low uranium concentrations (approximately 3.3 ppb), and serious biofouling damage, pose significant challenges in creating advanced materials that exhibit high stability, excellent adsorption performance, and superior selectivity [12,13]. Thus, it is imperative to focus on the development of high-performance adsorbent materials for the efficient extraction of uranium from seawater.

In recent years, metal-organic frameworks (MOFs) [14–18], porous aromatic frameworks (PAFs) [19–21] and porous organic polymers (POPs) [22–26] have garnered significant interest from researchers, and have been applied to uranium extraction from seawater. However, it is important to note that these materials often exhibit suboptimal performance in uranium extraction from seawater for one or more of the following reasons: slow kinetics, low adsorption capacities, and poor resistance to biofouling. Additionally, the synthesis of PAFs typically requires expensive catalysts, POPs often display disordered structures, and the frameworks of MOFs tend to collapse due to the dissociation of the coordination bond when subjected to prolonged soaking.

Covalent organic frameworks (COFs) possess designable structural diversity, high crystallinity, chemical stability, and excellent porosity, making them suitable for extensive applications in energy storage [27,28], catalysis [29–32], biomedicine [33–35], sensing [36–39], adsorption and separation [40–45]. Amidoxime-functionalized COFs have been shown to be effective in enriching uranium. For instance, COF-TpDb-AO can reduce the concentration of uranium in contaminated water from 1 ppm to 0.1 ppb, which is even lower than the standard for drinking water (30 ppb), while achieving an uptake capacity of 127 mg/g from uranium-spiked seawater [46]. The highly stable polyarelether-based COF (COF-HHTF-AO) demonstrates an adsorption capacity of 5.12 mg/g for uranium extraction from seawater [47]. However, the concentration of vanadium in seawater is the same order of magnitude as that of uranium, and amidoxime exhibits no significant selectivity for vanadium and uranium. Therefore, the design and synthesis of novel COF materials with specific coordination sites is imperative [48,49].

The synergistic adsorption strategy plays a significant role in enhancing the extraction of radionuclides [50]. Our group has reported the design and application of phosphonate-decorated hydrazone-linked COFs to remove radioactive UO_2^{2+} from highly acidic radioactive waste effectively. This effectiveness is attributed to the cooperative interactions between the framework's structural backbone and the side arms [51]. As one of the most commonly used pore surface engineering strategies for COFs, "thiol-ene" click reaction takes the advantages of versatility, high efficiency, mild reaction conditions, stable precursor structure in different solvents, appropriate pH values and temperatures to introduce active functional groups into the side arms of COFs with high efficiency and selectivity [52–55].

In this study, we report the synthesis of a vinyl-decorated hydrazone-linked covalent organic framework (COF), designated COF-IHEP5, which features hydrazone-carbonyl partner chelating sites [52]. This framework is subsequently modified through a "thiol-ene" click reaction to introduce hydrophilic carboxylic acid functional groups. By incorporating flexible carboxylic acid groups on the pore surface and synergistically embedding "uranium nanotraps" within the hydrazone-linked COF framework, the uranium adsorption capacity can be further enhanced. The maximum adsorption capacity of the post-modified COF-IHEP5-COOH for UO_2^{2+} has reached 543.8 mg/g, which is 1.5 times greater than that of the unmodified COF-IHEP5. Additionally, COF-IHEP5-COOH demonstrates an extraction efficiency of approximately 80 % for uranium from spiked natural seawater, including 4.5 times higher adsorption selectivity than vanadium. This work provides new insights and directions for the design of functionalized uranium adsorbents with excellent binding affinity and adsorption capacities.

To achieve the aforementioned goals, we designed and synthesized COF-IHEP5, in which the pore walls incorporate vinyl groups that facilitate subsequent chemical modifications. 2,5-Bis(allyloxy)terephthalohydrazide, as the important building block, was prepared through three steps in an overall yield of 78 % (more details are shown in synthetic procedure section in Supporting information). As shown in Fig. 1, the hydrazone-linked COF-IHEP5 was synthesized through the acid-promoted solvothermal method. Typically, 2,4,6-triformylphloroglucinol (TP) and vinyl-decorated 2,5-bis(allyloxy)terephthalohydrazide (BATH) were dis-

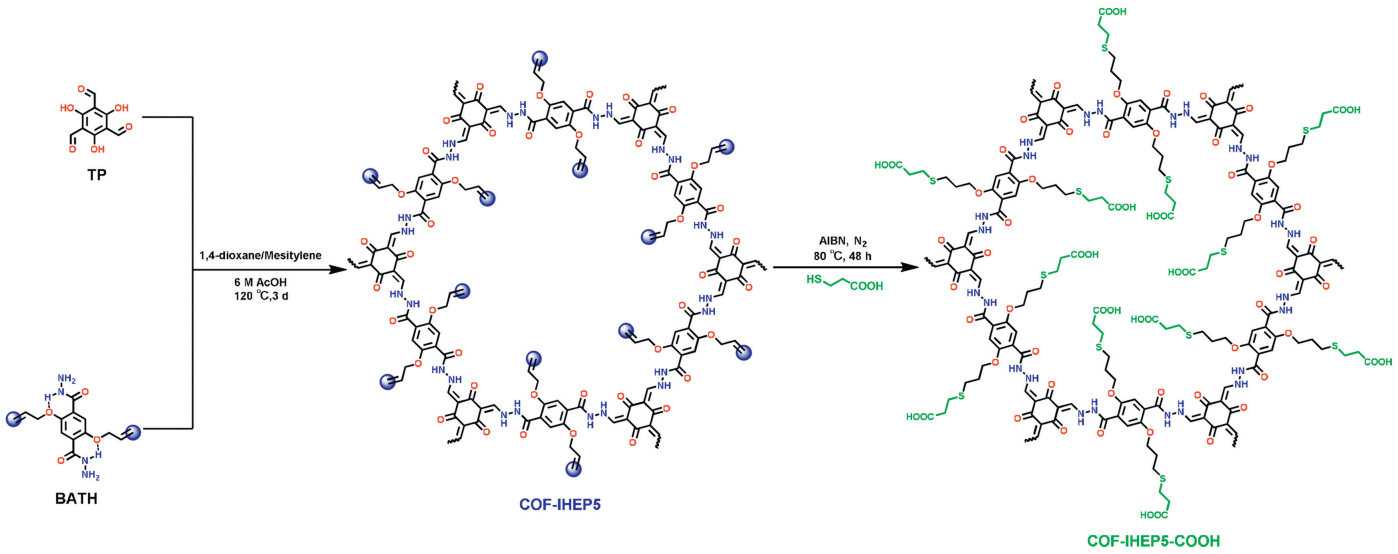


Fig. 1. Schematic diagrams for the synthesis and structure of COF-IHEP5 and COF-IHEP5-COOH post-modification by the "thiol−ene" click reaction.

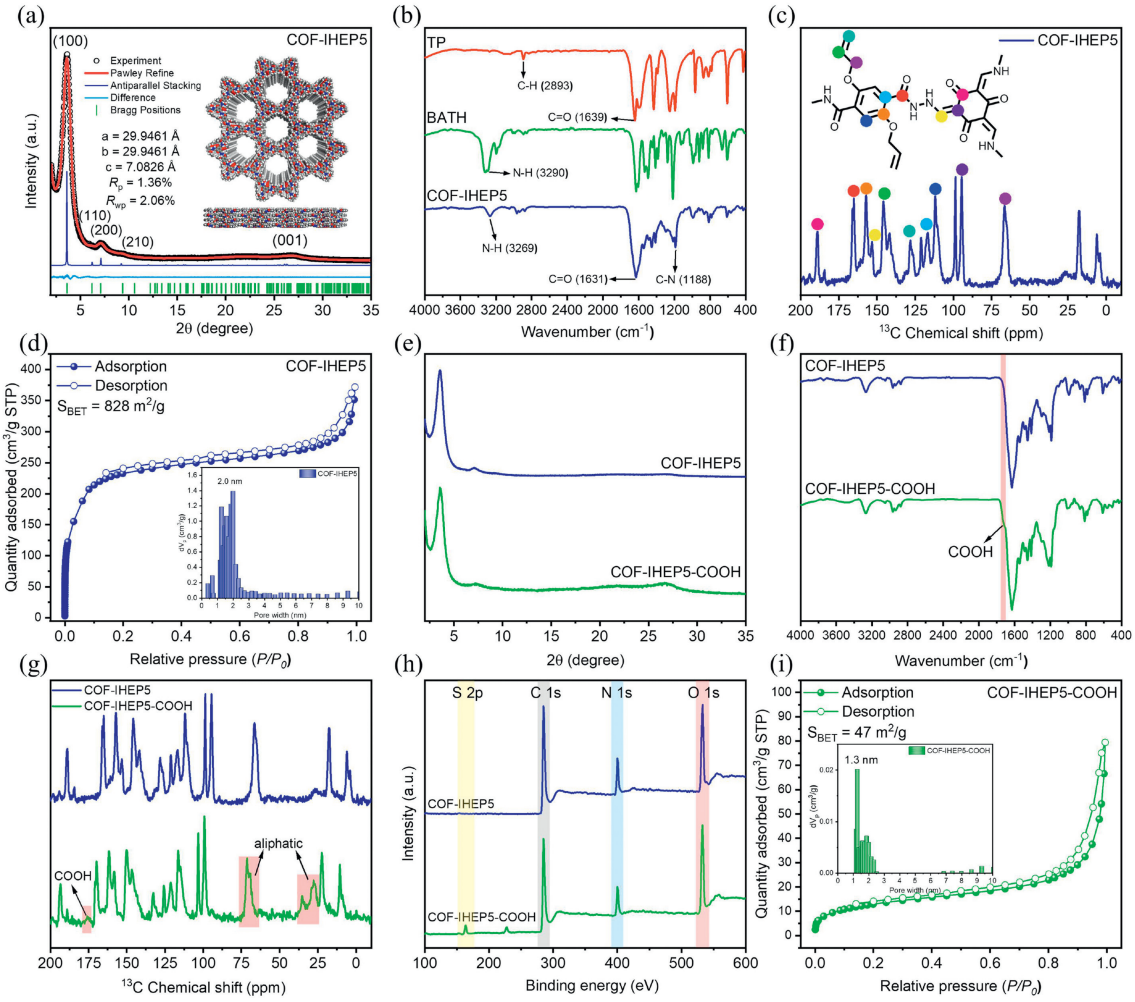


Fig. 2. (a) PXRD patterns of COF-IHEP5: experimental (black circle), Pawley refined (red), antiparallel stacking (blue), difference (aquamarine), and Bragg position (green). (b) FT-IR spectra comparison of TP (red), BATH (green) and COF-IHEP5 (blue). (c) Solid state ^{13}C CP/MAS NMR spectra of COF-IHEP5. (d) Nitrogen adsorption and desorption isotherms obtained from 77 K of COF-IHEP5; insets are the pore size distributions of COF-IHEP5. (e) PXRD patterns of COF-IHEP5 and COF-IHEP5-COOH. (f) FT-IR spectra of COF-IHEP5 and COF-IHEP5-COOH. (g) Solid state ^{13}C CP/MAS NMR spectra of COF-IHEP5 and COF-IHEP5-COOH. (h) XPS spectra of COF-IHEP5 and COF-IHEP5-COOH. (i) Nitrogen adsorption and desorption isotherms obtained from 77 K of COF-IHEP5-COOH; insets are the pore size distributions of COF-IHEP5-COOH.

persed in a mixed solvent of 1,4- dioxane/mesitylene (2 mL, 1:1) using AcOH (0.2 mL, 6 mol/L) as the catalyst at 120 °C for 3 days to give the yellow crystalline powder, which was used for further post-modification. Specifically, COF-IHEP5 was dispersed in 3-mercaptopropionic acid and 2,2-azobisisobutyronitrile *via* a "thiol−ene" click reaction at 80 °C for 48 h under N_2 atmosphere to obtain the carboxylic acid functionalized materials, which was designated as COF-IHEP5-COOH.

The crystallinity of COF-IHEP5 was determined by powder X-ray diffraction (PXRD) patterns and Pawley refinement analyses, and its structural properties were then further dissected by comparing experimental and simulation results. The PXRD pattern of COF-IHEP5 exhibited intense peaks at $2\theta = 3.61°$, 6.21°, 7.12°, 9.22°, and 26.39° (Fig. 2a), which could be readily assigned to diffraction on (100), (110), (200), (210), and (001) planes, respectively. Further Pawley refinements of simulation models towards the experimental PXRD patterns indicated that the unit cell of COF-IHEP5 crystallizes in the P6CC space group with $a = b = 29.9461$ Å, $c = 7.0826$ Å, $\alpha = \beta = 90°$, and $\gamma = 120.0°$ ($R_p = 1.36\%$, $R_{wp} = 2.06\%$) (Table S1 in Supporting information). To further verify the stacking structure of COF-IHEP5, we built three possible models, including eclipsed AA stacking model, staggered AB stacking model and the antiparallel AA stacking model. The experimental PXRD patterns of COF-IHEP5 compared with Materials Studio simulated patterns of different stacking modes indicated that the PXRD patterns matched well with the simulated antiparallel AA stacking model (Fig. S2 in Supporting information). As reported by Loh KP and co-workers [53,56,57], the intramolecular hydrogen bonding of the BATH linker plays a pivotal role in the orientation of the hydrazine groups on the linkers, thereby causing COF-IHEP5 to crystallize in the antiparallel AA stacking mode. In addition, the repulsion between alkyl oxygen atom of hydrazine groups in adjacent layers was expected to assist crystallization in the antiparallel AA stacking models [58,59]. The PXRD pattern of COF-IHEP5-COOH exhibited diffraction pattern comparable to that of COF-IHEP5 (Fig. 2e), indicating the preservation of excellent crystallinity after post-modification.

The Fourier transform infrared (FT-IR) spectra were obtained to verify the chemical structures and components. FT-IR spectra of COF-IHEP5 showed the presence of characteristic signal at ~1631 cm^{-1} corresponding to a lower energy characteristic of the carbonyl stretching vibration in the β-keto-enamine bond [51], while the N–H (3290 cm^{-1}) and C–H (2893 cm^{-1}) signals of the monomers almost disappeared, indicating the high polymerization of COF-IHEP5 (Fig. 2b). FT-IR spectra of COF-IHEP5-COOH showed the appearance of C=O of carboxylic acid stretching band at 1724

cm^{-1} (Fig. 2f) [53]. In addition, the preservation of the characteristic peak of β-keto-enamine bond at 1631 cm^{-1} further proved the retention of the chemical structure of COF-IHEP5 through the "thiol-ene" click reaction and demonstrated the excellent stability of COF-IHEP5.

The structural features of COF-IHEP5 and COF-IHEP5-COOH were further verified by solid-state ^{13}C cross-polarization magic angle spinning nuclear magnetic resonance (^{13}C CP/MAS NMR). As shown in Fig. 2c, the peaks at 188.8 and 165.1 ppm correspond to the carbon atoms of the carbonyl groups [52]. The peaks at 145.8, 128.1, and 66.4 ppm can be assigned to the allyl groups, which attached to the phenyl ring [60]. To ensure the successful connection of thiol species onto COF-IHEP5, the synthetic post-modified COF-IHEP5-COOH was characterized by ^{13}C CP/MAS NMR (Fig. 2g). The new peak at 175.8 ppm appears, which is assigned to the carbon in carboxyl group. The peaks at 71.3, 69.0, 35.4 and 27.8 ppm assigned to the aliphatic carbons, indicating that carboxylic acid was successfully anchored in COF-IHEP5-COOH [53]. Moreover, the X-ray photoelectron spectroscopy (XPS) of COF-IHEP5-COOH showed a new peak at 164 eV (Fig. 2h), which is assigned to S 2p that also evidencing the successful synthetically post-modification.

The inherent porosities of COF-IHEP5 and COF-IHEP5-COOH were investigated by N_2 adsorption−desorption isotherm curves at 77 K, and both COFs showed characteristic Type I shape. The Brunauer−Emmett−Teller (BET) surface areas of COF-IHEP5 and COF-IHEP5-COOH were calculated to be 828 and 47 m^2/g, and the pore volume were 0.49 and 0.08 cm^3/g, respectively. Pore size distribution analysis based on the nonlocal density functional theory (NLDFT) model exhibited that the pore size distributions of COF-IHEP5 and COF-IHEP5-COOH were centered at 2.0 and 1.3 nm, respectively (Figs. 2d and i), which match well with the antiparallel AA stacking structure (21.2 and 13.8 Å). The reduction in pore size also simultaneously validates the successful post-modification. The scanning electron microscopy (SEM) and transmission electron microscopy (TEM) show COF-IHEP5 and COF-IHEP5-COOH morphology of uniform porous nanofibers (Figs. S3-S6 in Supporting information). The stability and hydrophilicity of adsorbent materials have a decisive impact on their performance in practical applications. We first employed thermogravimetric analysis (TGA) to reveal the thermal stability of COF-IHEP5 and COF-IHEP5-COOH, both of which exhibited the high thermal stability, with <6% mass loss in air up to 300 °C (Figs. S7 and S8 in Supporting information). Chemical stability tests were performed by soaking the sample in aqueous HNO_3 (3 mol/L), aqueous NaOH (6 mol/L), DMF, THF and natural seawater, respectively, for one day. Radiolytic stability tests were conducted by exposing the sample to 50 kGy and 100 kGy doses of γ-rays environments. The FT-IR spectra and PXRD patterns of processed sample showed the retention of chemical and crystal structures, which reveal high irradiation stability of COF skeleton (Figs. S9 and S10 in Supporting information). Additionally, the water contact angle analysis demonstrated a much faster wetting process on the surface of COF-IHEP5-COOH in comparison to COF-IHEP5 (Figs. S11 and S12 in Supporting information), indicating that the embedding of carboxylic acid improves the hydrophilicity.

Batch experiments were performed to evaluate the uranium adsorption performances of COF-IHEP5 and COF-IHEP5-COOH in aqueous solutions, including the extraction efficiencies at different pH values, adsorption kinetics, adsorption capacities, the influences of competing ions, and recyclability [50,61,62]. Subsequently, we tested the uranium extraction ability of COF-IHEP5 and COF-IHEP5-COOH over a wide pH range, even in uranium-spiked natural seawater. The pH values of the aqueous solution significantly impact the uranyl existence forms and the chemical coordination of COFs with uranyl ions [63]. Under strong acid environment, a large number of O or N atoms in the functional groups are easily protonated in the presence of large amounts of H^+, which results in a significant decrease in adsorption performance of COFs. Besides, under strongly alkaline environment, OH^- and CO_3^{2-} will coordinate with U(VI), which also causes a serious decline for uranium adsorption capacity on COFs. Therefore, the adsorption efficiency at different pH values is an important indicator for evaluating uranium adsorbents. We tested the uranium extraction efficiencies of COF-IHEP5 and COF-IHEP5-COOH at a wide pH ranging from 2 to 9 with the initial concentration of 20 mg/L. As shown in Fig. 3a, at pH of 3–9, COF-IHEP5-COOH exhibits powerful extraction efficiencies over 99% towards uranium, the high efficiency at pH 8 implies the potential ability in uranium extraction from seawater. It is worth noting that COF-IHEP5-COOH is obviously superior to COF-IHEP5 towards uranium adsorption at the pH 2–4, which confirms the advantage of synergistic effect. Considering uranium extraction efficiency of two adsorbents at different pH values and the influence of uranyl ion precipitation at high pH values, we conducted subsequent adsorption experiments at pH 5.

In addition to affecting the chemical coordination, the pH value of uranium solution also affects the surface charge distribution of COFs leading to electrostatic attraction and electrostatic repulsion phenomena. We measured the zeta potential values of COF-IHEP5 and COF-IHEP5-COOH at pH values ranging from 2 to 9 (Fig. 3b). COF-IHEP5 and COF-IHEP5-COOH have an isoelectric point at pH 3 to pH 4, whereas COF-IHEP5-COOH is more negatively charged in aqueous solution due to the deprotonation of –COOH group around pH 3 to pH 5 [63]. This is one of the reasons why the adsorption capacity of COF-IHEP5-COOH is better than that of COF-IHEP5 at low pH. On the contrary, when the pH is below 3, COF-IHEP5 and COF-IHEP5-COOH will be protonated and positively charged, which causes the significant decrease in adsorption capacity under highly acidic conditions.

As shown in Fig. 3c, we investigated the functional relationship between uranium adsorption quantity (q_t) and contact time (t) in an uranium aqueous solution with an initial concentration of 50 mg/L at pH 5. The adsorption behaviors of COF-IHEP5 and COF-IHEP5-COOH fit well with the *pseudo*-second-order kinetics model with high coefficient of determination (R^2) of 0.995 and 0.999 (Fig. S13 and Table S2 in Supporting information), which are higher than those of the pseudo-first-order kinetics model (0.977 and 0.939). Therefore, the adsorption driving force of COF-IHEP5 and COF-IHEP5-COOH for uranyl can be attributed to chemisorption. COF-IHEP5 and COF-IHEP5-COOH take about 48 h to reach adsorption equilibrium.

As shown in Fig. 3d, the adsorption capacities (q_e) of COF-IHEP5 and COF-IHEP5-COOH were explored through the adsorption isotherms at pH 5 and initial concentrations ranging from 20 mg/L to 300 mg/L. The Langmuir and Freundlich fitting models were used to study the sorption behaviors of uranyl ions on COF-IHEP5 and COF-IHEP5-COOH. Both the adsorption isotherms of COF-IHEP5 and COF-IHEP5-COOH were found to fit better with the Langmuir fitting model with high coefficient of determination (R^2) of 0.982 and 0.996 (Fig. S14 and Table S3 in Supporting information), which are higher than those of the Freundlich fitting model (0.957 and 0.893), indicating a monolayer sorption mechanism. The maximum adsorption capacities of COF-IHEP5 and COF-IHEP5-COOH calculated by the Langmuir equation, are 352.3 mg/g for COF-IHEP5 and 543.8 mg/g for COF-IHEP5-COOH, which exhibits a significant enhancement of adsorption capacities through carboxylic acid post-modification strategy. Meanwhile, COF-IHEP5-COOH shows excellent uranium absorption capacity comparing to previously reported COF adsorbents (Table S4 in Supporting information).

Uranium adsorption and desorption tests were conducted to evaluate the reusability of the adsorbent. Uranyl ions were released from COF-IHEP5 and COF-IHEP5-COOH using 1 mol/L Na_2CO_3 aqueous solution as the eluent. As shown in Fig. 3e, after five cy-

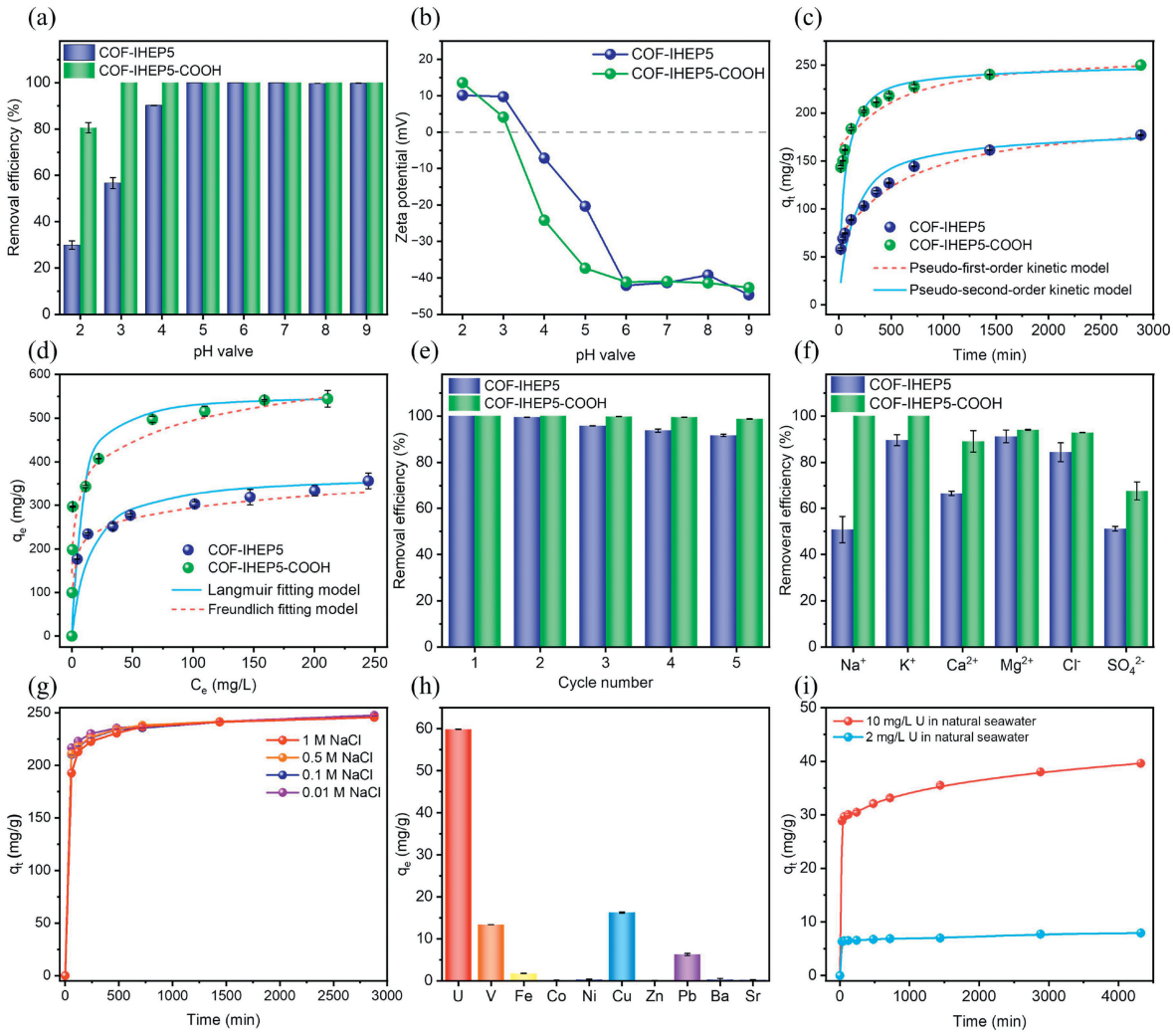


Fig. 3. Uranium extraction properties of COF-IHEP5 and COF-IHEP5-COOH. (a) Effect of pH on the uranium adsorption efficiency. (b) Zeta potentials depending on pH values in aqueous solution. (c) Sorption kinetics curves fitting with the *pseudo*-second-order model. (d) Adsorption isotherms fitting with the Langmuir model. (e) Extraction efficiencies in five adsorption/desorption cycles. (f) Influence of high concentration (0.2 mol/L) coexisting cations and anions on the uranium adsorption efficiency. (g) Influence of different NaCl concentration on the uranium adsorption efficiency. (h) Selectivity of COF-IHEP5-COOH in the simulated seawater containing different competing cations. (i) Uranium extraction performances of COF-IHEP5-COOH in uranium-spiked natural seawater.

cles of adsorption and desorption, the extraction efficiency remains greater than 95 %. In addition, the crystallinity and chemical structure of the adsorbent were retained after five cycles, which were evidenced by PXRD and FT-IR data (Figs. S15 and S16 in Supporting information). These results indicate that both COF-IHEP5 and COF-IHEP5-COOH have excellent uranium extraction regenerability.

The selectivity of the adsorbent is a crucial factor, which greatly affect the extraction efficiency, especially facing numerous interfering ions and high ion concentration in the real seawater environment. Therefore, we first evaluated the effects of co-existing cations (K^+, Na^+, Mg^{2+} and Ca^{2+}) and anions (Cl^- and SO_4^{2-}) which have the highest concentration in seawater. As shown in Fig. 3f, COF-IHEP5-COOH maintained high adsorption efficiency even in the presence of high concentrations of coexisting ions. On the contrary, the adsorption capacity of COF-IHEP5 decreased significantly under the influence of high concentration ions, demonstrating the excellent contribution of carboxylic acid through the post-modification method for uranium extraction. Considering the high salt content in seawater, the adsorption experiment for uranium was conducted at different salt concentration. As shown in Fig. 3g, neither the adsorption kinetics nor the maximum adsorption capacity of COF-IHEP5-COOH was affected.

The selectivity of COF-IHEP5-COOH for U(VI) was further investigated in real seawater containing 0.05 mmol/L UO_2^{2+}, and 0.05 mmol/L of eight competitive ions including transition metal and rare earth cations. As shown in Fig. 3h, COF-IHEP5-COOH demonstrated outstanding performance for selective extraction of U(VI) with a high removal efficiency of 99 %. The distribution coefficient (K_d) of COF-IHEP5-COOH for U(VI) was calculated to be 1.8×10^6 mL/g. Besides that, the selectivity for uranium is 4.5 times greater than that for vanadium, as evidenced by the K_d (U)/K_d (V) ratio, and the selectivity for other competing ions is markedly superior. This enhanced affinity of COF-IHEP5-COOH for uranium, compared to high concentration interfering ions, underscores its promising potential for the recovery of uranyl from seawater.

The adsorption kinetics of uranium on COF-IHEP5-COOH were investigated in real seawater with the addition of 10, 2, 1, and 0.1 mg/L uranium. As shown in Fig. 3i, both kinetic curves fit well with the *pseudo*-second-order model, with high coefficient of determination (R^2) of 0.998 and 0.999. And the equilibrium adsorption capacities were 8.12 mg/g and 40.32 mg/g for 2 mg/L and 10 mg/L, respectively, demonstrating a high extraction efficiency of approximately 80 % for uranium from spiked natural seawater. When uranium concentration was at the ppb level, COF-IHEP5-

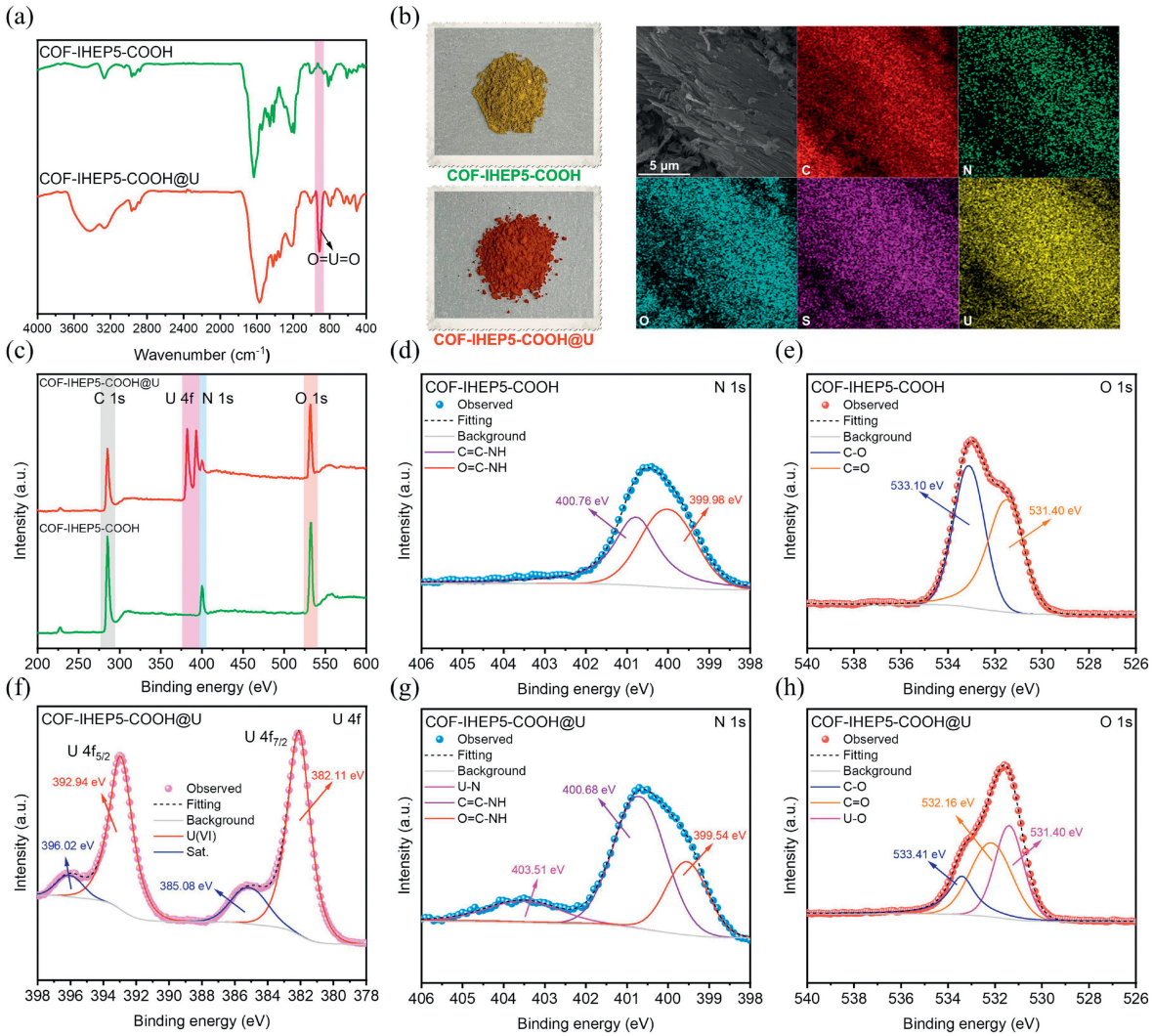


Fig. 4. (a) FT-IR spectra of COF-IHEP5-COOH and COF-IHEP5-COOH@U. (b) Digital photos of COF-IHEP5-COOH and COF-IHEP5-COOH@U, and SEM-EDS Mapping of COF-IHEP5-COOH@U. (c) The full XPS spectra of COF-IHEP5-COOH and COF-IHEP5-COOH@U. (d) N 1s high-resolution XPS spectra of COF-IHEP5-COOH. (e) O 1s high-resolution XPS spectra of COF-IHEP5-COOH. (f) U 4f high-resolution XPS spectra of COF-IHEP5-COOH@U. (g) N 1s high-resolution XPS spectra of COF-IHEP5-COOH@U. (h) O 1s high-resolution XPS spectra of COF-IHEP5-COOH@U.

COOH remained the high adsorption efficiency (Fig. S17 in Supporting information), indicating its potential application value in the real seawater environment. In addition, the crystallinity and chemical structure of COF-IHEP5-COOH remained after treating it with natural seawater for 7 days, as further evidenced by PXRD and FT-IR analysis (Fig. S18 in Supporting information). These results indicate that COF-IHEP5-COOH has excellent chemical stability in seawater.

PXRD, FT-IR, SEM-EDS Mapping and XPS analysis were performed to further elucidate the detailed adsorption mechanism of U(VI) by both COF-IHEP5 and COF-IHEP5-COOH. After uranium extraction, the color of COF-IHEP5 changed from yellow to orange-red, and the color of COF-IHEP5-COOH changed from green to dark red (Fig. S19 in Supporting information). PXRD and FT-IR studies were conducted to characterize COF-IHEP5, COF-IHEP5@U, COF-IHEP5-COOH, and COF-IHEP5-COOH@U. The PXRD patterns of COF-IHEP5@U and COF-IHEP5-COOH@U indicate that they still maintain a high degree of crystallinity (Fig. S20 in Supporting information). In addition, as shown in FT-IR spectra of COF-IHEP5@U and COF-IHEP5-COOH@U, an intense characteristic peak at 912 cm^{-1} could be ascribed to the *anti*-symmetric stretching vibration of O=U=O (Fig. 4a and Fig. S21a in Supporting information). The SEM-EDS mapping of COF-IHEP5@U and COF-IHEP5-COOH@U (Fig. 4b and Fig. S21b in Supporting information) indicates that U(VI) was adsorbed on COF-IHEP5 and COF-IHEP5-COOH.

XPS studies were performed to deeply understand the interaction mechanism between the two adsorbents (COF-IHEP5 and COF-IHEP5-COOH) and uranium species. As shown in Fig. 4c, the XPS survey spectra all exhibit characteristic peaks at ~285, ~400, and ~533 eV assignable to C 1s, N 1s, and O 1s, respectively. As shown in Fig. 4f, the high-resolution XPS spectra of U 4f exhibited strong peaks, giving the U $4f_{5/2}$ and U $4f_{7/2}$ binding energies at 392.9 and 382.1 eV for COF-IHEP5-COOH@U, respectively, which are significantly lower than those of $UO_2(NO_3)_2{\cdot}6H_2O$ (393.4 eV and 382.5 eV) [46]. These results indicate that uranium species maintained the U(VI) valence state during the adsorption process, and that there are strong interactions between the uranium species and COF-IHEP5-COOH. A comparison of the high-resolution C 1s XPS spectra of COF-IHEP5-COOH and COF-IHEP5-COOH@U revealed that the fitted C=O signal shifted from 287.91 eV to 288.26 eV [64]. In addition, the high-resolution N 1s XPS spectrum of COF-IHEP5-COOH@U (Figs. 5d and g) exhibited a new peak at 403.51 eV as compared to that of COF-IHEP5-COOH, which was ascribed to the U-N signal peak [36,65,66]. The high-resolution O 1s XPS spec-

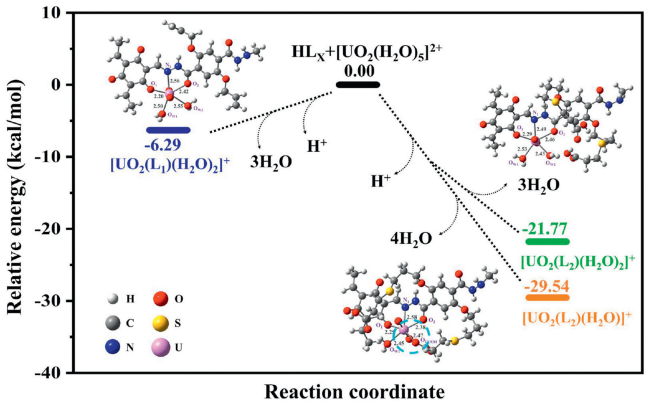


Fig. 5. Structural models and binding energies (kcal/mol) of COF-IHEP5 (HL_1), COF-IHEP5-COOH (HL_2) with uranyl cations calculated by DFT. The C, N, O, S, U, and H atoms are represented by gray, blue, red, yellow, pink, and white spheres, respectively.

tra of COF-IHEP5-COOH@U (Figs. 5e and h) appeared a new peak at 531.40 eV compared to that of COF-IHEP5-COOH, which revealing the U-O signal peak [36,47,65–67], and the C-O and C=O signal peaks shifted from 533.10 eV and 531.40 eV to 533.41 eV and 532.16 eV. The high-resolution XPS spectra of COF-IHEP5 and COF-IHEP5@U displayed the same results (Fig. S21 in Supporting information). All the XPS spectra indicate strong interactions between U(VI) and O and N in the acylhydrazide carbonyl adsorption sites of COFs.

To explore the roles of the assisting functional groups and hydrazine-carbonyl chelating sites in the uranium adsorption process, density functional theory (DFT) calculations were used to calculate the adsorption energy of uranyl cations by different COFs (COF-IHEP5 and COF-IHEP5-COOH). We employed a condensed COFs unit as the simulation model consisting of a hydrazine linker and a TP molecule, where L_1 and L_2 denote the models of COF-IHEP5 and COF-IHEP5-COOH, respectively. The hydrazine-carbonyl chelate sites in L_1 and L_2 can coordinate with uranyl cations to form $[UO_2(L_1)(H_2O)_2]^+$ and $[UO_2(L_2)(H_2O)_2]^+$ complexes. In addition, L_2 can participate in uranyl cations coordination not only through the hydrazine-carbonyl chelating site but also *via* oxygen derived from the deprotonation of the carboxyl group located on the flexible branch of the side arms, leading to the formation of the $[UO_2(L_2)(H_2O)]^+$ complex. The calculated results are shown in Fig. 5. For the condensed COFs units, the calculated binding energies for $[UO_2(L_1)(H_2O)_2]^+$, $[UO_2(L_2)(H_2O)_2]^+$, $[UO_2(L_2)(H_2O)]^+$ were −6.29, −21.77, and −29.54 kcal/mol, respectively. This indicates that the affinity of COF-IHEP5-COOH for uranyl cations is stronger than that of COF-IHEP5. In addition, the coordination of the carboxyl groups in COF-IHEP5-COOH enhances the binding energy. Therefore, COF-IHEP5-COOH is more likely to adsorb uranyl cations compared to COF-IHEP5, which is consistent with the experimental results. The synergistic coordination of the carboxyl groups in COF-IHEP5-COOH is more able to enhance the affinity for uranyl cations and thereby improving its adsorption performance for uranyl cations.

In summary, this work reports a carboxylic acid-functionalized COF for highly efficient extraction of uranium from seawater. Using pore surface engineering, we successfully modified the carboxylic acid group into the pores of COF-IHEP5. The developed COF-IHEP5-COOH demonstrated good stability, high adsorption capacity, and recyclability toward uranium under complex conditions. The maximum adsorption capacity of the post-modified COF-IHEP5-COOH for UO_2^{2+} reached 543.8 mg/g, which is 1.5 times greater than that of the unmodified COF-IHEP5. After five adsorption cycles, the efficiency remains above 98 %. Additionally, COF-IHEP5-COOH demonstrates an extraction efficiency of approximately 80 % for uranium from spiked natural seawater with a U/V adsorption mass ratio of 4.5. The DFT calculations show that COF-IHEP5-COOH adsorbent, with tailor-made binding sites bearing a strong affinity promotes highly efficient extraction of uranium from seawater. This study presents a novel strategy for designing functional materials with enhanced affinity for uranium extraction from seawater. Further work to fabricate more effective COFs for uranium extraction from seawater by introducing other tailor-made functional groups on the side-arm of COFs skeleton is in progress.

Declaration of competing interests

The authors declare that they have no known competing financial interests or personal relationships that could have appeared to influence the work reported in this paper.

CRediT authorship contribution statement

Junjie Yu: Writing – review & editing, Writing – original draft, Visualization, Validation, Methodology, Formal analysis, Data curation, Conceptualization. **Yichen Huang:** Visualization, Software, Methodology, Formal analysis. **Pengcheng Zhang:** Validation, Methodology, Formal analysis, Conceptualization. **Shusen Chen:** Supervision, Project administration, Funding acquisition. **Yan Song:** Supervision, Project administration, Funding acquisition. **Congzhi Wang:** Visualization, Software, Methodology, Formal analysis. **Zijie Li:** Supervision, Resources. **Liyong Yuan:** Supervision, Resources, Funding acquisition. **Jipan Yu:** Writing – review & editing, Validation, Supervision, Resources, Methodology, Funding acquisition. **Nannan Wang:** Supervision, Resources, Funding acquisition. **Weiqun Shi:** Writing – review & editing, Supervision, Project administration, Funding acquisition.

Acknowledgment

This work was supported by the Project of Uranium Extraction from Seawater (No. HNKF202216(36)).

Supplementary materials

Supplementary material associated with this article can be found, in the online version, at doi:10.1016/j.cclet.2025.111378.

References

[1] J. Chilvers, R. Bellamy, H. Pallett, et al., Nat. Energy 6 (2021) 250.
[2] S. Chu, A. Majumdar, Nature 488 (2012) 294.
[3] M. Hoffert, K. Caldeira, G. Benford, et al., Science 298 (2002) 981.
[4] N. Kaltsoyannis, S. Liddle, Chem 1 (2016) 659.
[5] R. Taylor, Chem 1 (2016) 662.
[6] Y. Yue, R. Mayes, G. Gill, et al., RSC Adv. 5 (2015) 50005.
[7] R. Davies, J. Kennedy, R. Mcilroy, et al., Nature 203 (1964) 1110.
[8] J. Xiong, S. Hu, Y. Liu, et al., ACS Sustain. Chem. Eng. 5 (2017) 1924.
[9] Y. Xie, Z. Liu, Y. Geng, et al., Chem. Soc. Rev. 52 (2023) 97.
[10] D. Zhang, L. Fang, L. Liu, et al., Sep. Purif. Technol. 320 (2023) 124204.
[11] Y. Wu, Y. Xie, X. Liu, et al., Coord. Chem. Rev. 483 (2023) 215097.
[12] Z. Wang, R. Ma, Q. Meng, et al., J. Am. Chem. Soc. 143 (2021) 14523–14529.
[13] Y. Yuan, Q. Meng, M. Faheem, et al., ACS Cent. Sci. 5 (2019) 1432–1439.
[14] L. Chen, Z. Bai, L. Zhu, et al., ACS Appl. Mater. Interfaces 9 (2017) 32446–32451.
[15] Y. More, S. Mollick, S. Saurabh, et al., Small 20 (2024) 2302014.
[16] J. Wu, N. Shi, N. Li, et al., ACS Appl. Mater. Interfaces 15 (2023) 46952–46961.
[17] Y. Yuan, S. Feng, L. Feng, et al., Angew. Chem. Int. Ed. 59 (2020) 4262–4268.
[18] Q. Yu, Y. Yuan, J. Wen, et al., Adv. Sci. 6 (2019) 1900002.
[19] B. Li, Q. Sun, Y. Zhang, et al., ACS Appl. Mater. Interfaces 9 (2017) 12511–12517.
[20] D. Chen, Y. Li, X. Zhao, et al., ACS Cent. Sci. 9 (2023) 2326–2332.
[21] Z. Wang, Q. Meng, R. Ma, et al., Chem 6 (2020) 1683–1691.
[22] Q. Sun, Y. Song, B. Aguila, et al., Adv. Sci. 8 (2021) 2001573.
[23] Y. Song, C. Zhu, Q. Sun, et al., ACS Cent. Sci. 7 (2021) 1650–1656.
[24] L. Zhang, N. Pu, B. Yu, et al., ACS Appl. Mater. Interfaces 12 (2020) 3688–3696.
[25] Q. Sun, B. Aguila, J. Perman, et al., Nat. Commun. 9 (2018) 1644.

[26] Z. Zhong, Y. Huang, W. Yang, Ind. Chem. Mater. 3 (2025) 57–68.
[27] C. Zhang, J. Xie, C. Zhao, et al., Adv. Mater. 35 (2023) 2304511.
[28] X. Xu, S. Zhang, K. Xu, H, et al., J. Am. Chem. Soc. 145 (2023) 1022–1030.
[29] Y. Zhong, W. Dong, S. Ren, et al., Adv. Mater. 36 (2024) 2308251.
[30] Y. Yang, H. Zhang, Y. Wang, et al., Adv. Mater. 35 (2023) 2304170.
[31] J. Cheng, Y. Wu, W. Zhang, et al., Adv. Mater. 35 (2023) 2305313.
[32] Y. Fu, Y. Gao, H. Jia, et al., Green Energy Environ 10 (2025) 804–812.
[33] L. Zhang, S. Wan, J. Zhang, et al., J. Am. Chem. Soc. 145 (2023) 17689–17699.
[34] L. Zhang, A. Song, Q. Yang, et al., Nat. Commun. 14 (2023) 5355.
[35] Y. Liu, L. Yuan, W. Chi, et al., Nat. Commun. 15 (2024) 7150.
[36] W. Cui, C. Zhang, W. Jiang, et al., Nat. Commun. 11 (2020) 436.
[37] W. Cui, Y. Chen, W. Xu, et al., Sep. Purif. Technol. 306 (2023) 122726.
[38] C. Niu, C. Zhang, W. Cui, et al., J. Hazard. Mater. 425 (2022) 127951.
[39] C. Liu, C. Jia, S. Gan, et al., Chin. Chem. Lett. 35 (2024) 109750.
[40] D. Cao, F. Cui, C. Zhang, et al., Adv. Funct. Mater. (2024) 2413729.
[41] Y. Wang, J. Lan, X. Yang, et al., Adv. Funct. Mater. 32 (2022) 2205222.
[42] Y. Wang, M. Xie, J. Lan, et al., Chem 6 (2020) 2796–2809.
[43] G. Li, Y. Wu, C. Zhong, et al., Chin. Chem. Lett. 35 (2024) 108904.
[44] J. Li, G. Chen, C. Chen, et al., Chin. Chem. Lett. 36 (2025) 109760.
[45] W. Chen, M. Li, W, et al., Green Energy Environ. 7 (2022) 296–306.
[46] Q. Sun, B. Aguila, L.D. Earl, et al., Adv. Mater. 30 (2018) 1705479.
[47] G. Cheng, A. Zhang, Z. Zhao, et al., Sci. Bull. 66 (2021) 1994–2001.
[48] Y. Xie, Y. Wu, X. Liu, et al., Cell Rep. Phys. Sci. 4 (2023) 101220.
[49] Y. Yuan, D. Cao, F. Cui, et al., Nat. Water 3 (2025) 89–98.
[50] J. Yu, L. Yuan, S. Wang, et al., CCS Chem. 1 (2019) 286–295.
[51] J. Yu, J. Lan, S. Wang, et al., Dalton Trans. 50 (2021) 3792–3796.
[52] B. Yao, J. Li, N. Huang, et al., ACS Appl. Mater. Interfaces 10 (2018) 20448–20457.
[53] X. Li, Q. Hou, W. Huang, et al., ACS Energy Lett. 5 (2020) 3498–3506.
[54] M. Guo, X. Guan, Q. Meng, et al., Angew. Chem. Int. Ed. (2024) e202410097.
[55] M. Li, L. Chen, J. Du, et al., ACS Appl. Mater. Interfaces 16 (2024) 8688.
[56] X. Li, J. Qiao, S. W, et al., J. Am. Chem. Soc. 142 (2020) 4932–4943.
[57] X. Li, J. Qiao, S. Quek, et al., ACS Mater. Lett. 2 (2020) 654–657.
[58] Y. Xie, Q. Rong, C. Wen, et al., CCS Chem. 6 (2023) 1908–1919.
[59] Y. Xie, Q. Rong, F. Mao, et al., Nat. Commun. 15 (2024) 2671.
[60] H. Yang, M. Hao, Y. Xie, et al., Angew. Chem. Int. Ed. (2023) e202303129.
[61] S. Wang, L. Wang, Z. Li, et al., J. Hazard. Mater. 408 (2021) 124949.
[62] H. Tu, Y. Wu, Z. Li, et al., Chem. Eng. J. 485 (2024) 150089.
[63] Z. Li, R. Zhu, P. Zhang, et al., Chem. Eng. J. 434 (2022) 134623.
[64] X. Liu, X. Wang, W. Jiang, et al., Chem. Eng. J. 450 (2022) 138062.
[65] F. Li, W. Cui, W. Jiang, et al., J. Hazard. Mater. 392 (2020) 122333.
[66] W. Cui, F. Li, R. Xu, et al., Angew. Chem. Int. Ed. 59 (2020) 17684–17690.
[67] C. Niu, C. Zhang, X. Liu, et al., Nat. Commun. 14 (2023) 4420.